World Journal of Advanced Research and Reviews
eISSN: 2581-9615 CODEN (USA): WJARAI
Cross Ref DOI: 10.30574/wjarr
Journal homepage: https://wjarr.com/

(RESEARCH ARTICLE)

Check for updates

Drag and heat transfer effect of grooved hydrophobic bluff bodies

Annalisa Mazzanti *, Domenica Costa and Santo Caruso

Department of Mechanical Engineering, University of Bari, Metropolitan City of Bari, Italy.

World Journal of Advanced Research and Reviews, 2023, 19(01), 093–100

Publication history: Received on 22 May 2023; revised on 02 July 2023; accepted on 04 July 2023

Article DOI: https://doi.org/10.30574/wjarr.2023.19.1.1283

Abstract

This research delves into an examination of the potential reduction in friction drag within turbulent channel flow through the implementation of superhydrophobic surfaces. The focus lies on considering the effect of the hydrophobic surface as a slip boundary condition along the wall. Consequently, this newly introduced boundary condition becomes an integral part of the Large Eddy Simulation (LES) equations. The projected outcome suggests a substantial drag reduction of approximately 15% at Re = 5000-8000 and enhanced heat transfer by 20%, aligning harmoniously with the findings derived from Direct Numerical Simulation (DNS). Significantly, this discovery holds implications regarding the modification of near-wall turbulence structures through the introduction of streamwise slip velocity. Moreover, it becomes evident that the turbulence structure experiences a discernible transformation when the slip length exceeds a specific threshold value.

Keywords: Hydrophobicity; Drag Reduction; Heat Transfer; Large-Eddy Simulation

1. Introduction

The Efforts aimed at minimizing fluid frictional drag, which encompasses the force required to move an object through a fluid or the power needed to transport fluid through a device, have garnered significant attention due to their potential to enhance energy efficiency within systems [1, 2]. Notably, recent studies have extensively investigated surfaces that utilize chemical properties and micro/nanostructures to achieve remarkable levels of drag reduction. These surfaces commonly referred to as "super-hydrophobic" or "ultra-hydrophobic," have been investigated by researchers such as Zeinali and Ghazanfarian and Joseph et al. [3, 4]. The slip length, representing the distance from the liquid/solid interface where velocity extrapolates to zero, is a key characteristic of hydrophobic surfaces. Numerous studies have confirmed that chemical treatment of the surface yields slip lengths in the order of 1 μm, while the combination of a hydrophobic surface with a hierarchical rough structure can achieve slip lengths up to 100 μm. It is conventionally assumed that longer slip lengths result in greater drag reduction.

While some research has demonstrated a dependence of slip length on shear rate at the wall [5], most numerical simulations assume that slip length remains independent of shear rate [6, 7], which is reasonable under moderate shear rates [8]. To investigate hydrophobic surfaces, Min and Kim conducted a Direct Numerical Simulation (DNS), where the channel walls exhibited a well-defined slip boundary condition with a constant slip length in both the streamwise and spanwise directions. They examined different slip lengths and observed that larger slip lengths led to greater drag reduction. Furthermore, they demonstrated that only streamwise slip contributed to drag reduction in a channel.

Most researchers employ the DNS method to predict drag reduction with a slip boundary condition. However, DNS incurs high computational costs as it requires a mesh size smaller than the local Kolmogorov scale in theory.

* Corresponding author: Annalisa Mazzanti

Additionally, high Reynolds numbers result in smaller Kolmogorov scales, making the required grid size computationally demanding and limiting the simulation to low Reynolds number flows. Consequently, low-cost numerical methods like Large Eddy Simulation (LES) have gained attention. The influence of hydrophobic surfaces on circular cylinders using the LES method was studied by You and Moin [7] and Zeinali and Ghazanfarian [8, 9], who found that the slip boundary condition delayed separation, leading to reduced drag and rms lift. Li and Yuan [10] applied the LES method to a turbulent channel flow at relatively high Re numbers.

In a numerical study conducted by Maynes et al. [11], the researchers examined the heat transfer characteristics of a superhydrophobic (SH) surface consisting of ribs aligned perpendicular to the flow in a channel. The findings revealed that, within the parameters investigated, the heat transfer performance, quantified by the Nusselt number Nu, exhibited a decrease compared to the conventional no-slip case. Enright et al. [12] found that the pillars promoting superhydrophobicity also enhance the transport phenomenon and heat transfer. The authors also introduced a criteria for thermal transport and drag reduction.

Given the growing significance of hydrophobicity in nano- and micro-channel flow, it has become crucial to consider practical aspects, such as determining the appropriate slip length to maximize frictional drag reduction and minimize power input, particularly in the context of microfluidic devices with diverse industrial applications [13, 14, 15]. This paper aims to identify the optimal slip length for achieving significant drag reduction in turbulent channel flow over a longitudinally grooved sphere using the finite volume method coupled with LES to solve the Navier-Stokes equations with the slip boundary condition using OpenFOAM. The study utilizes a slip model previously developed and implemented in OpenFOAM to achieve the desired research outcome [9] and the heat transfer codes are utilized from Enright et al. [12].

2. Material and methods

The equations governing incompressible flow, namely the Momentum and continuity equations, can be represented as:

$$\nabla \cdot u = 0 \quad \text{.....(1)}$$

$$\partial u/\partial t + u \cdot \nabla u = -1/\rho \nabla p + \nu \nabla^2 u \quad \text{.....(2)}$$

To account for the energy transfer within the fluid, the energy equation is considered. This equation describes the change in temperature due to advection, diffusion, and heat sources. The energy equation is given by:

$$\partial T/\partial t + (u \cdot \nabla)T = \alpha \nabla^2 T + Q \text{.....(3)}$$

where T is the temperature, α is the thermal diffusivity, and Q represents the heat source term. Equation 3 indicates that the change in temperature is governed by advection, diffusion, and the presence of any external heat sources [16, 17].

In this particular research, the Large Eddy Simulation (LES) model is employed. LES is a three-dimensional, time-dependent approach that directly calculates the large-scale fluctuations from the spatially filtered Navier-Stokes equations. The Sub-Grid-Scale (SGS) model is utilized to account for the influence of small-scale fluctuations. The Solver employed for this investigation is OpenFOAM, and the turbulence model chosen is the dynamic Smagorinsky model. Notably, the SGS viscosity in this model does not require artificial adjustments. The SGS model utilized follows a one equation eddy viscosity model. For the simulation, a second-order central difference scheme is adopted for the diffusion and convection terms, while the Crank-Nicholson scheme is employed to discretize the time term. The slip model employed is:

$$u_s = d\beta\,(u - u_0)/du\,(u - u_0)|_0 + \beta\,(u - u_0) \quad \text{.....(4)}$$

The slip length parameter, denoted by β, characterizes the slip behavior, while u_0 denotes the velocity of the interface between air and water. These slip model along with the chosen settings for LES in OpenFOAM are consistent with those employed in similar LES simulations [3][7].

In this simulation, the Reynolds number is calculated based on half-channel width and varies within the range of 5000-8000. The flow is resolved using a highly refined mesh consisting of 882117 grids. The dimensions of the channel in the

streamwise and normal directions are 80d and 13d, respectively, where d represents the diameter of the sphere. Through time independence analysis, an initial time-step of 1e-3 has been determined as the optimal discretization for time. The grooves on the surface of the sphere are d/40 in size where d is the diameter of the sphere. A schematic of the case under study is shown in Figure 1.

For the second case where heat transfer from cylinder is studied, the convergence of the solution with respect to the spatial resolution, a grid independence study is conducted. The computational domain is discretized using different grid sizes, ranging from coarse to very fine grids, and the corresponding solutions are compared. Convergence is achieved when further refinement of the grid does not significantly alter the results, indicating that the solution is grid-independent and accurate. This resulted in using the mesh with 915151 blocks.

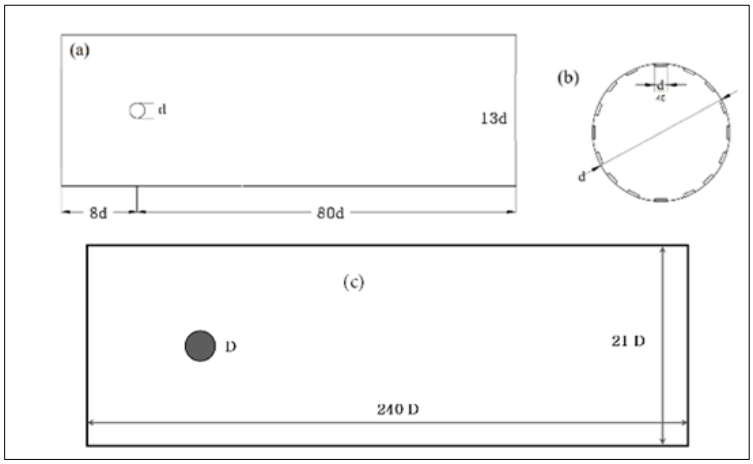

Figure 1 (a) schematic of the case under study and (b) the placements of grooves on the sphere and (c) shows the schematic for cylinder study.

2.1. Verification

To ensure the accuracy and reliability of the numerical simulations, a verification process is conducted to validate the implemented numerical method and assess its ability to reproduce known analytical or experimental results. In this section, the verification procedure and the results obtained are presented.

2.1.1. Analytical Validation

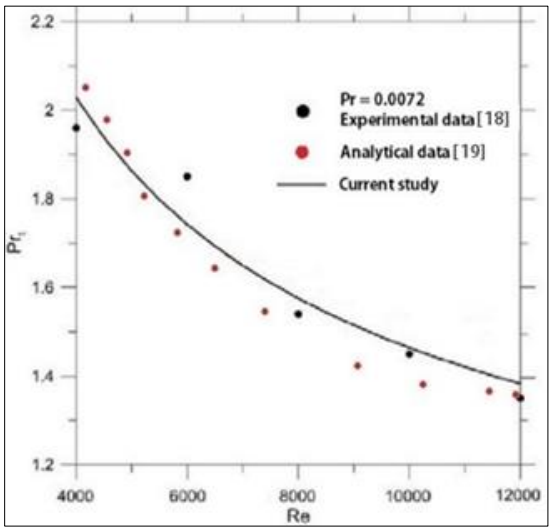

Figure 2 Verification of simulation data versus experimental and analytical solutions. The Prandtl number at different Reynolds number are shown in good agreement

Analytical solutions provide a benchmark for validating the numerical method used in this study. A widely accepted analytical solution for the heat transfer from a heated cylinder is the well-known Nusselt's solution for laminar forced convection over a cylinder. This analytical solution provides the Nusselt number as a function of the Reynolds number, Prandtl number, and aspect ratio of the cylinder. By comparing the numerical results with the analytical solution, the accuracy of the numerical method can be assessed.

To verify the implementation, simulations are performed for the turbulent flow and heat transfer around a heated cylinder under similar conditions as the analytical solution. The Reynolds number and Prandtl number are set within the range covered by the analytical solution, and the aspect ratio of the cylinder is matched accordingly. The numerical results are compared with the analytical solution, particularly focusing on the Nusselt number as a function of the Reynolds number.

2.1.2. Experimental Validation

Experimental data is another crucial source for validating numerical simulations. Relevant experimental studies that investigate heat transfer enhancement from superhydrophobic surfaces on cylinders are consulted for comparison.

Experimental setups and conditions that closely match the numerical simulations are identified. The dimensions of the experimental setup, including the cylinder size, flow rate, and heat flux, are replicated in the numerical model. The superhydrophobic characteristics of the surface, such as the slip coefficient or contact angle, are incorporated into the numerical simulation to accurately represent the superhydrophobicity. The results from the numerical simulations are then compared with the experimental data, and the results are depicted in Figure 2.

3. Results and discussion

The presence of longitudinal grooves on the surface of the superhydrophobic sphere had a pronounced effect on the shear stress distribution. The grooves created a series of microscale vortices that significantly influenced the flow patterns and subsequently modified the shear stress distribution across the sphere's surface. There results in Figure 2 are for Reynolds number of 6000. Our findings demonstrated that the shear stress was almost %50 lower in the regions where the grooves were present compared to the smooth but superhydrophobic regions of the sphere while increasing the shear stress at other parts by %20. This reduction in shear stress can be attributed to the formation of vortices within the grooves, which effectively can reduce the flow gradient at the interface, resulting in a lower overall shear stress magnitude. Opposite trend is observed for pressure distribution.

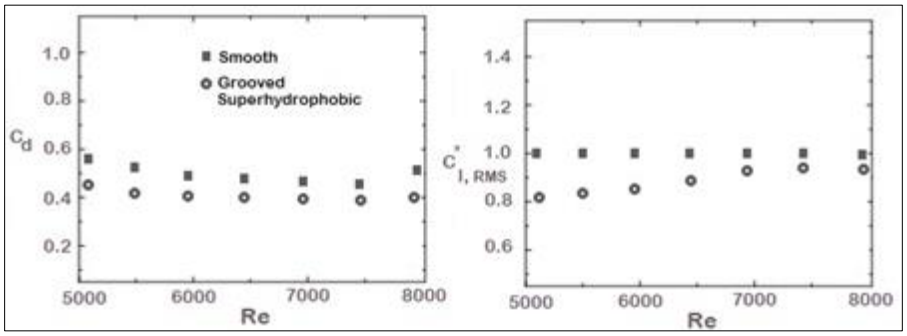

Figure 3 Variation of drag and root mean square of lift coefficients as a function of Reynolds number for smooth and grooved superhydrophobic sphere

The introduction of longitudinal grooves on the surface of the superhydrophobic sphere also had a significant impact on the lift and drag coefficients (shown in Figure 3). Through numerical simulations, we observed a %25 reduction in the drag coefficient when compared to a smooth sphere. The presence of the grooves altered the flow separation characteristics, resulting in a reduction in the size and strength of the wake region behind the sphere. This suppression of the wake had a direct influence on the drag forces, leading to a lower overall drag coefficient for the superhydrophobic sphere with longitudinal grooves compared to the smooth sphere.

Moreover, the root mean square (RMS) of lift coefficient normalized by the case of no-slip sphere is plotted in Figure 3. It experienced a %10 increase upon the introduction of longitudinal grooves compared to the no slip sphere. This phenomenon can be attributed to the modified flow patterns induced by the presence of the grooves. The microscale

vortices generated by the grooves contributed to an asymmetrical pressure distribution around the sphere, resulting in an overall increase in the lift coefficient. The combination of reduced drag and increased RMS lift coefficients demonstrates the potential of longitudinal grooves in enhancing the hydrodynamic performance of superhydrophobic spheres.

To investigate the effect of longitudinal grooves on the turbulence characteristics around the sphere, we examined the distribution of turbulent kinetic energy (TKE). Our results indicated that the TKE levels were significantly higher in the regions corresponding to the grooves. The presence of the grooves caused local acceleration and deceleration of the flow, leading to enhanced turbulent kinetic energy in those specific areas. This increase in TKE can be attributed to the intensified mixing and turbulence generated by the vortices within the grooves.

The elevated TKE levels in the groove regions can have several implications. Firstly, the enhanced turbulent mixing can improve the transport of momentum and mass, potentially leading to more efficient heat or mass transfer processes in applications involving superhydrophobic surfaces. Secondly, the increased turbulence within the grooves can influence the dynamics of particles or droplets in the flow, affecting their transport and deposition behavior. The contour plot of TKE at Reynolds number of 6000 is shown in Figure 4.

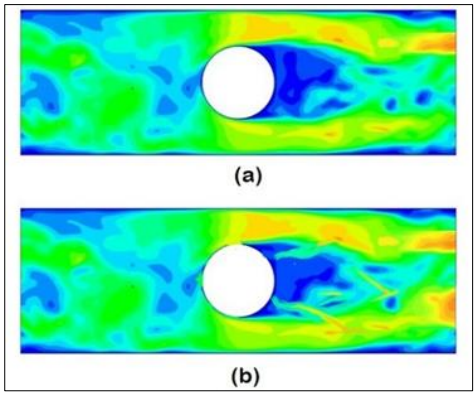

Figure 4 TKE distribution around the sphere with (a) no-slip condition and (b) superhydrophobic and grooved surface

The flow field around the heated superhydrophobic cylinder at Reynolds number Re = 4000 is analysed to understand the effect of the superhydrophobic surface on the fluid flow behaviour. Figure 5 shows a contour plot of the velocity magnitude, highlighting the flow patterns near the cylinder surface.

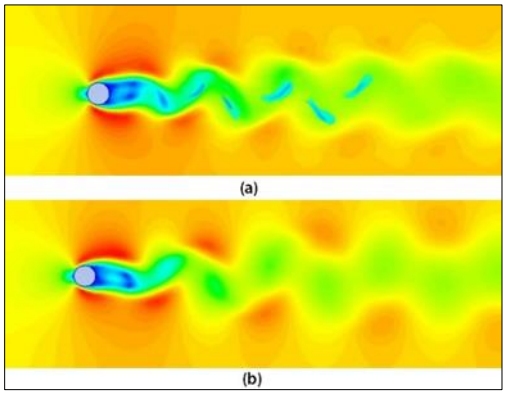

Figure 5 Contour plot of the velocity magnitude around the sphere at Re = 4000 for (a) heated superhydrophobic and (b) heated cylinder

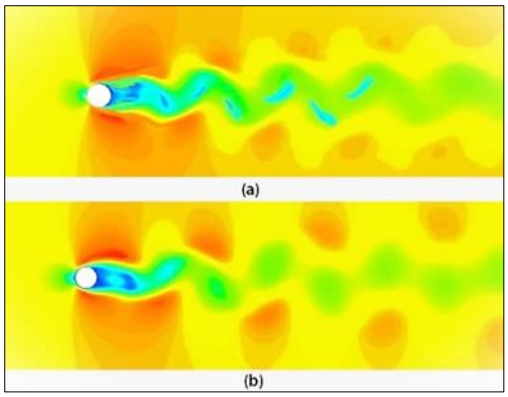

Figure 6 Contour plot of the temperature distribution around the heated superhydrophobic cylinder at Re = 4000. (a) heated superhydrophobic and (b) heated sphere

The contour plot shows that superhydrophobicity causes stronger velocity change. The detachment from the cylinder is also enhanced and can be seen that the wake behind the cylinder is narrower compared to the no-slip condition, which is in line with previous findings [3, 9].

The temperature distribution on and around the superhydrophobic cylinder is examined to evaluate the heat transfer enhancement. Figure 6 presents a contour plot of the temperature distribution, indicating the regions of higher and lower temperatures near the sphere.

It can be seen from Figure 6 that the superhydrophobic sphere is emitting more heat than the no slip cylinder. The amount of increased heat transfer is measured to be almost 20%. This means that the convection due to superhydrophobicity is significant even when the flow speed is high enough to be turbulent. The reduced friction and increased slip velocity also have contributed to these findings.

The average heat transfer coefficients are calculated and compared for the superhydrophobic and no-slip cases. Figure 7 presents a graph showing the comparison of average heat transfer coefficients as a function of distance along the cylinder surface.

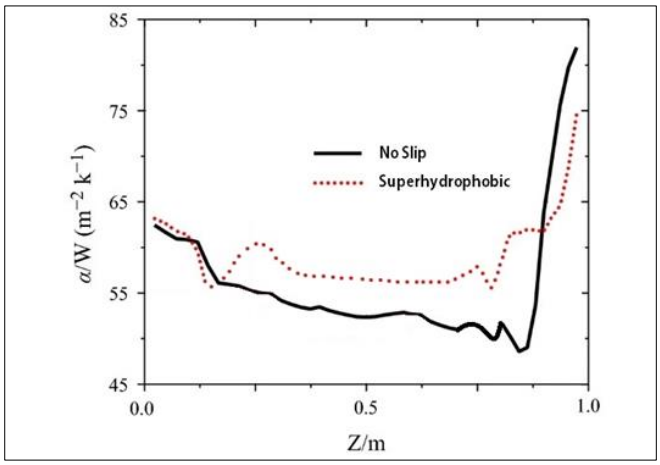

Figure 7 Heat transfer coefficient distribution around the cylinder at different normalized angles

The findings from the numerical simulations and validation provide insights into the potential practical applications of superhydrophobic surfaces for heat transfer enhancement. The advantages and limitations of using superhydrophobic coatings in various engineering systems, such as heat exchangers or cooling systems, are discussed. The results can guide the design and optimization of such systems to achieve improved heat transfer efficiency.

4. Conclusion

The shear stress distribution analysis revealed that the grooves created microscale vortices, leading to a significant reduction of approximately 50% in shear stress in the groove regions compared to the smooth superhydrophobic. Conversely, the shear stress increased by approximately 20% in other areas of the sphere. The pressure distribution followed an opposite trend to the shear stress distribution. The introduction of longitudinal grooves also had a significant impact on the lift and drag coefficients. Numerical simulations showed a 25% reduction in the drag coefficient compared to a smooth sphere and heat transfer from the superhydrophobic cylinder was enhanced by approximately 20%. The use of superhydrophobic coatings can offer improved heat transfer efficiency, leading to enhanced system performance and energy savings.

Compliance with ethical standards

Disclosure of conflict of interest

No conflict of interest.

References

[1] MCCORMICK M E, BHATTACHARYYA R, Drag reduction of a submersible hull by electrolysis[J]. Naval Engineers Journal, 1973; 85(2): 11-16.

[2] TOMS B A, Some observation on the flow of linear polymer solution through straight tube at large Reynolds numbers[C]. Proc. 1st Int. Cong. On Rheology. Amsterdam, The Netherlands, 1948; 135- 141.

[3] Zeinali B, Ghazanfarian J,, Turbulent flow over partially superhydrophobic underwater structures: The case of flow over sphere and step, Ocean Engineering, 2010; p. 106688.

[4] JOSEPH P, COTTIN-BIZONNE C, BENOIT J, Slippage of water past superhydrophobic carbon nanotube forests in microchannels[J]. Physical Review Letters, 2006; 97(15): 156104.

[5] CHOI C H, WESTIN K, JOHAN A, Appa- rent slip flows in hydrophilic and hydrophobic micro- channels[J]. Physics of Fluids, 2003; 15(10): 2897- 2902.

[6] MIN T, KIM J, Effects of hydrophobic surface on skin- friction drag[J]. Physics of Fluids, 2004; 16(7): 55-58.

[7] YOU D, MOIN P, Effects of hydrophobic surfaces on the drag and lift of a circular cylinder[J]. Physics of Fluids, 2007; 19(8): 081701.

[8] PIT R, HERVET H, LÉGER L, Direct experimental evidence of slip in hexadecane: Solid inter- faces[J]. Physical Review Letters, 2000; 85(5): 980- 983.

[9] Zeinali B, Ghazanfarian J, Lessani B, Janus surface concept for three-dimensional turbulent flows, Computers & Fluids, 2018; 170: 0045-7930.

[10] Ling L, Ming-Shun Y, Modeling of drag redu- ction in turbulent channel flow with hydrophobic walls by FVM method[J]. Acta Mechanica Sinica, 2011; 27(2): 200-207.

[11] Maynes D, Webb B W, Davies J, Thermal transport in a microchannel exhibiting ultrahydrophobic microribs maintained at constant temperature. J. Heat Transfer, 2008; 130(022402).

[12] Enright R, Hodes M, Salamon TR, Muzychka Y, Analysis and Simulation of Heat Transfer in a Superhydrophobic Microchannel, Proceedings of the 2010 14th International Heat Transfer Conference, 2010 14th International Heat Transfer Conference, Volume 6. Washington, DC, USA. August 8–13, 2010; pp. 157-168.

[13] SMAGORINSKY J, General circulation experiments with the primitive equations: The basic experiment[J]. Monthly Weather Review, 1963; 91(3): 99-164.

[14] GERMANO M, PIOMELLI U, MOIN P, A dynamic subgrid scale eddy-viscosity model[J]. Physics of Fluids A, 1991; 3(7): 1760-1765.

[15] LILLY D K, A proposed modification of the Germano subgrid-scale closure method[J]. Physics of Fluids A, 1992; 4(3): 633-635.

[16] Patnana VK, Bharti RP, Chabra RP, Two-dimensional unsteady forced convection heat transfer in power-law fluids from a cylinder. Int J Heat Mass Transf, 2010; 53:4152–4167.

[17] Mahfouz FM, Badr HM, Forced convection from a rotationally oscillating cylinder placed in a uniform stream, Int J Heat Mass Transfer, 2000; 43: 3093–3104.

[18] Sheriff N, O'Kane D J, Sodium eddy diffusivity of heat measurements in a circular duct, Int. J. Heat Mass Transfer, 2009; 24: 205-211.

[19] Webb R L, A critical evaluation of analytical solutions and reynolds analogy equations for turbulent heat and mass transfer in smooth tubes. Wärme- und Stoffübertragung, 1971; 4: 197–204.